Phys. Status Solidi B **247**, No. 8, 2033–2039 (2010) / **DOI** 10.1002/pssb.200983961

physica status solidi b
www.pss-b.com
basic solid state physics

Metal–insulator transition in Si(111)-(4 × 1)/(8 × 2)-In studied by optical spectroscopy

E. Speiser*[,1], S. Chandola[1,2], K. Hinrichs[1], M. Gensch[3], C. Cobet[1], S. Wippermann[4], W.G. Schmidt[4], F. Bechstedt[6], W. Richter[6], K. Fleischer[2], J. F. McGilp[2], and N. Esser[1]

[1] Leibniz-Institut für Analytische Wissenschaften – ISAS – e.V., Albert-Einstein-Str. 9, 12489 Berlin, Germany
[2] School of Physics, Trinity College Dublin 2, Ireland
[3] Helmholtz Zentrum Berlin, Germany
[4] Theoretische Physik, Universität Paderborn, Germany
[5] Institut für Festkörpertheorie und -Optik, Friedrich-Schiller-Universität, Jena, Germany
[6] Dipartimento di Fisica, Università di Roma Tor Vergata, Via della Ricerca Scientifica 1, 00133 Roma, Italy

Received 16 March 2010, revised 24 March 2010, accepted 1 April 2010
Published online 18 June 2010

Keywords metal–insulator transitions, optical properties, Raman spectroscopy, surface structures

* Corresponding author: e-mail eugen.speiser@isas.de, Phone: +49-30 6392-3552, Fax: +49-30 6392-3544

Measurements of the surface vibrational modes and optical response of Si(111)-(4 × 1)/(8 × 2)-In are compiled and a comparison to *ab initio* calculations performed within DFT-LDA formalism is given. Surface resonant Raman spectroscopy allows identifying a number of surface phonons with high spectral precision. The phase transition of the (4 × 1)–(8 × 2) surface structure is found to be accompanied by characteristic changes of the surface phonons, which are discussed with respect to various structural models suggested. The optical anisotropy of the (8 × 2) phase shows that the anisotropic Drude tail of the (4 × 1) phase is replaced by two peaks at 0.50 and 0.72 eV. The spectroscopic signatures of the (4 × 1) and (8 × 2) phases agree with a metal–insulator transition. The mid-IR-anisotropic optical response of the insulating (8 × 2) phase is interpreted in terms of electronic single particle excitations between surface electronic bands related to the In-nanowire surface. Comparison of the measured optical transitions with DFT *ab initio* calculations for the hexagon model and the trimer model of the (8 × 2) structure shows evidence for the existence of the hexagon structure.

1 Introduction Submonolayer coverages of metals on vicinal semiconductor surfaces often form chain structures showing localized 1-D electronic states which can be controlled on an atomic scale. The probably most intensively studied system of this kind is the ordered array of In nanowires. In the last years a commonly accepted structural model [Fig. 1(a)] was established by experiment and theory for the nanowire room temperature (RT) phase. In this model the nanowires consist of two In zigzag chains ordered in a (4 × 1) periodicity. The nanowires are separated by Si chains resembling the π-bonded chains of the clean Si(111)(2 × 1) surface. The surface structure models are shown in Fig. 1 for the RT phase (4 × 1) and low temperature (LT) phase (4 × 2) reconstructions, according to a commonly accepted model calculation [1]. The LT phase is achieved mainly by an alternating displacement of the In atoms towards their neighbours in the same chain. The (8 × 2) structure follows in this model from the (4 × 2) structure if the pair wise displacement of In atoms, as indicated by arrows in Fig. 1(b), is shifted by half a lattice constant along [1$\bar{1}$0] in adjacent In zigzag-chains. An alternative model for the In nanowires LT phase was suggested in Ref. [2]. In this model the surface structure consists no longer of chains but isolated 'clusters' where the central part of the 'cluster' is formed by a hexagonal-like arrangement of In atoms [Fig. 4(a)].

The geometry of such reconstructions is often controversial because of small 'real space' differences which make distinguishing between such reconstructions difficult experimentally using, *e.g.*, LEED and STM. Also from a theoretical point of view, the assignment of the real space structure is often difficult due to very small differences in

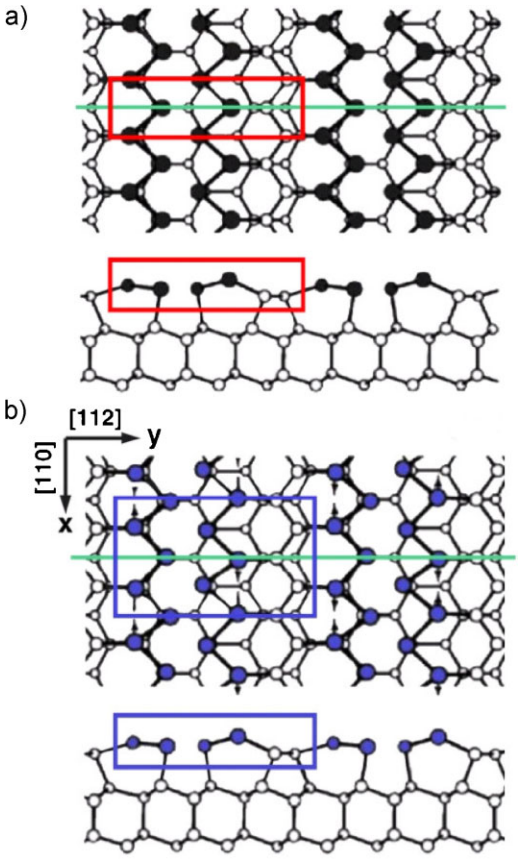

Figure 1 (online colour at: www.pss-b.com) Schematics of the (4 × 1) (a) and (4 × 2) (b) surface structures according to the model of Wang et al. [1]. Both reconstructions form a zigzag-chain like arrangement of the In atoms along the [110] crystal direction in Si substrate. The unit cells are marked by the red and blue boxes. The horizontal green line displays the orientation of the mirror plane, perpendicularly oriented to the surface. The displacement of In atoms in the (4 × 2) reconstruction in respect to the (4 × 1) reconstruction is marked by arrows. The so called 'trimer' formation consists of tree adjacent In atoms with shorter bond lengths within the In chains.

calculated total energies which can be in the range of the numerical and systematic errors.

The vibrational properties of a material are closely related to its atomic structure and therefore could be used to investigate surface reconstructions. High resolution electron energy loss spectroscopy (HREELS) [3, 4] and helium atom scattering (HAS) [5–7] are standard tools for surface vibrational spectroscopy. Raman spectroscopy has in recent years been successfully applied to probe surface phonons [8–12]. Much of the Raman work on surface vibrational modes concerns clean and Sb-terminated (110) surfaces of III–V semiconductors. Surface vibrations of Sb terminated III–V(110) surfaces were compared to *ab initio* phonon calculations performed by different theoretical approaches to test the validity of the model approximations [12]. Accordingly, surface resonant Raman spectroscopy can be used to study surface structure formation on semiconductor surfaces [13]. In particular the accurate Raman frequencies as well as the Raman selection rules are linked to the surface structure and thus are valuable to validate different competing structural models.

Moreover, the electronic and therefore the optical properties are very sensitive to small structural changes associated with different models of the reconstruction.

Reflectance anisotropy spectroscopy (RAS) is an optical surface specific technique which makes anisotropic optical transitions accessible. As can be seen from the reconstruction model in Fig. 1 the In/Si surface is highly anisotropic because of the chain like structure. Moreover, the fact that the Si bulk structure is O_h excludes any significant contribution to the RAS signal from the substrate bulk.

In this paper, we review Raman modes recorded on the In-nanowires on Si(111) (4 × 1) and (8 × 2), the two reconstructions known to occur at RT and LT. The surface phonon modes are discussed with respect to available other experimental and theoretical results, in particular with regard to the controversial discussion of the atomic structure of the (8 × 2) reconstruction. The resonant behaviour of the RT Raman modes is also addressed. A comparison of surface transitions revealed by RAS and *ab initio* electronic band structure calculations is also presented. This comparison supports the suggested 'hexagonal' reconstruction of the In terminated Si(111) surface.

2 Experimental methods The Raman measurements were performed using a setup in near back scattering geometry attached to a UHV vessel. A schematics of the setup is shown in Fig. 2. The measurements were performed at a base pressure of 8×10^{-11} mbar. The UHV vessel was equipped with a liquid helium cooling stage with integrated direct current heating, a Knudsen cell for In evaporation, LEED, AES, STM and optical windows. Vicinal Si(111) with an off cut of 1° towards [$\overline{1}$12] was used. The formation of the single domain (4 × 1) surface and the (4 × 1)–(8 × 2) surface phase transition was monitored *in situ* with RAS [14]. RAS measures the difference in reflectance, at near

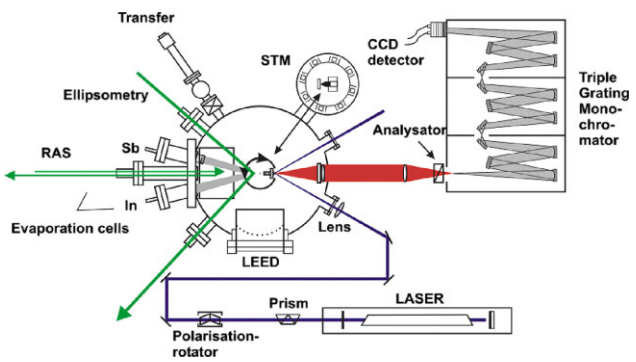

Figure 2 (online colour at: www.pss-b.com) Experimental Raman-UHV setup. A triple grating monochromator and Ar/Kr-ion lasers are used. The sample is placed inside a UHV vessel which is equipped with heating and cooling facilities, LEED, STM, evaporation sources and additional windows for ellipsometry and RAS.

normal incidence, of light linearly polarized in two orthogonal directions at the surface plane of a cubic material. With a three-domain surface of equal statistical weight, no anisotropy would be observed because of domain averaging. Consequently, the amplitude of the RAS signal is maximum if the surface is single domain [14]. Deposition at 400 °C was monitored by RAS and controlled by maximizing the main In-related RAS feature at 2 eV. After cooling to RT, LEED patterns showed a single domain (4 × 1) reconstruction.

3 Results and discussion

3.1 Optical surface anisotropy The In-nanowire terminated Si surface gives rise to distinct electronic states. Optical transitions in the surface are revealed by RAS spectra, as shown in Fig. 3. The data reveal a smooth increase to low energy for the RT (4 × 1) phase, while the LT (8 × 2) phase shows two sharp positive peaks at 0.50 and 0.72 eV. Positive anisotropy indicates that optical transitions with dipole momentum parallel to the chains are dominant in this spectral region. The strong optical absorption bands in the spectral range between 1.8 and 2.1 eV for both phases

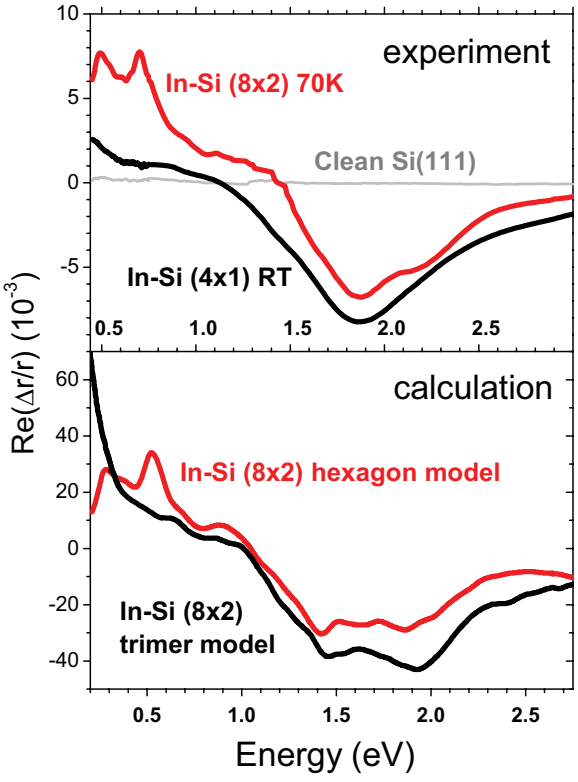

Figure 3 (online colour at: www.pss-b.com) Top panel: experimental RAS spectra for (8 × 2)-(LT) and (4 × 1)-(RT) phases. Lower panel: calculations for the (8 × 2)-(LT) phase based on trimer and hexagon models. A resonance is seen at 1.8 eV and only slightly distinct features for the (4 × 1)-(RT) and (8 × 2)-(LT) surface phases in the visible range. Two additional peaks appear at 0.5 and 0.72 eV for the (8 × 2) phase. While both calculations, based on trimer and hexagon models, agree well with experiment above 0.7 eV, the hexagon structure resembles the new transitions below 0.7 eV.

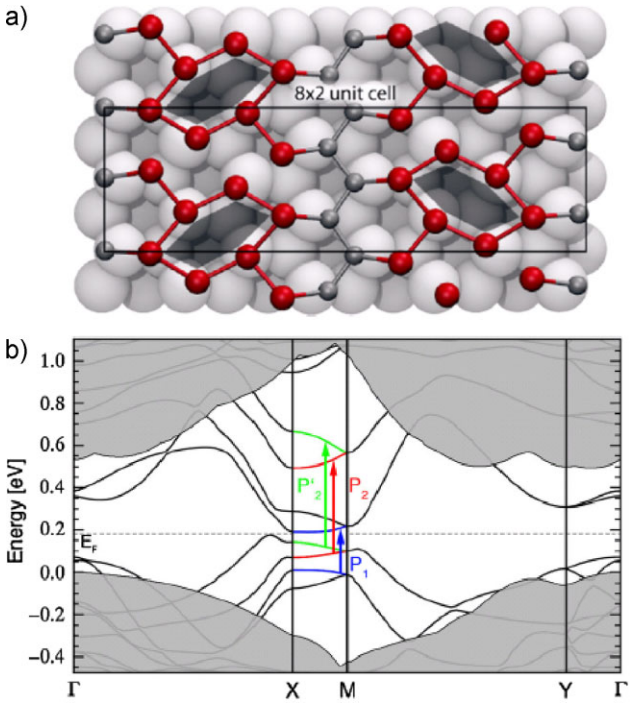

Figure 4 (online colour at: www.pss-b.com) (a) Hexagonal reconstruction model (hexagon formation is marked by shaded polygons) and (b) the electronic band structure of the hexagon model for In/Si(111)-(8 × 2)-In calculated within DFT-LDA (from Ref. [17]). Pronounced optical transitions showing up in the RAS spectra are marked. Grey regions correspond to the projected Si bulk bands. The bulk valence band maximum is chosen as energy zero. The Fermi level is indicated.

correspond to electronic transitions between surface states which are well below the direct E_1 optical gap of bulk Si. The negative anisotropy around 2 eV is related to a multitude of optical transitions having a dipole momentum perpendicular to the In chain direction that are either related to pure In chain states or involve the In–Si bonds. The former occur around 1.9 eV whereas the latter are observed at energies slightly above 2 eV. However, it is not directly related to the metallicity of the nanowires, which at low frequencies is expected to result in a stronger optical coupling for light polarized in the chain direction rather than perpendicularly to the chains. Therefore, the quasi one-dimensional metallicity of the In chains should lead to positive optical anisotropies, which are indeed observed for photon energies below 1 eV. The metallicity of the (4 × 1) RT phase and trimer (4 × 2) LT distorted chain model is supported by calculations of electronic band structures [15]. The optical transitions below 1 eV can be explained in terms of a hexagonal reconstruction model shown in Fig. 4(a).

Calculations of RAS spectra, based on this model, were performed using density functional theory (DFT) within the local density approximation (LDA) for exchange and correlation in Ref. [16]. The slab polarizability in the independent-particle approximation was utilized and no adjustable parameters were used. The calculated anisotropy

of both the trimer and hexagon models of the (8×2) structure agree well with the experiment above 0.7 eV.

Below 0.7 eV, only the hexagon model looks similar to the experimental results. In particular, two positive peaks are predicted, separated by 0.24 eV. This splitting agrees very well with the experimental splitting of 0.22 eV. The origin of the two peaks in the mid IR can be traced to optical transitions close to the M point of the surface Brillouin zone (SBZ), indicated by P_1 and $P_2 = P_2'$ in Fig. 4(b). Around M, nearly parallel valence and conduction bands close to the Fermi level give rise to a high joint density of states. From the orbital character of states (not shown here) we can assign P_1 to transitions between bonding and non-bonding In chain states within the single In zigzag chains, while P_2 and P_2' involve in addition In–In bonds between the two parallel zigzag chains. These bonds are characteristic for the hexagon model [Fig. 4(a)] and allow thus to relate the measured mid-IR data directly related to the structure of the In nanowire array. Detailed comparison reveals that the calculated mid-IR peaks are red-shifted by 0.25 eV (note the different scales in Fig. 3). The underestimation of excitation energies is typical for DFT calculations where self-energy effects are neglected. The complexity and size of the In nanowire structure prevents the calculation of optical spectra using many-body perturbation theory that includes self-energy and excitonic effects [18]. Quasiparticle calculations for the high-symmetry points of the hexagon model surface band structure found self-energy effects to increase the lowest transition energies by 0.26 eV on average [19]. A larger shift of 0.5 eV, typical for Si excitation energies [18], applies to the higher energy negative optical anisotropies, because the optical transitions involve Si states [16]. Allowing for these energy shifts, a very good agreement is found between the calculated (hexagonal model) and measured RAS spectra. The comparison between RAS measurements and theoretical calculations for 'chain' and 'hexagon' reconstruction models strongly support the hexagonal model.

3.2 Raman selection rules As a result of symmetry considerations the Raman selection rules determine for which polarization of incoming and scattered light a certain phonon mode is Raman active or inactive ('allowed' or 'forbidden'). The selection rules are given as Raman tensors which are tabulated for all irreducible presentations of the crystallographic point groups [20]. Silicon crystals (diamond structure) belong to the point group O_h. For Raman backscattering on the (111) surfaces the principal axes of light polarization are the $[1\bar{1}0]$ and the $[11\bar{2}]$ crystal directions. Deformation potential scattering of the bulk TO mode is then symmetry allowed in any polarization configuration, *i.e.* for polarizations of incident and scattered light (E_i, E_s) along $([1\bar{1}0],[11\bar{2}])$, along $([1\bar{1}0],[1\bar{1}0])$ and along $([11\bar{2}],[11\bar{2}])$, respectively [20].

Different selection rules apply for the surface phonon modes, since the termination of the 3D-crystal imposes a symmetry reduction. A (4×1) single domain indium nanowire terminated Si(111) belongs to the point group C_S. The corresponding normal modes separate into A' and A'' surface modes which are symmetry allowed under parallel or perpendicular polarization configurations, respectively [11]. The Raman tensors in the coordinate system $x = [1\bar{1}0]$, $y = [11\bar{2}]$ are given by [11]:

$$\mathbf{R}(A') = \begin{pmatrix} a & 0 \\ 0 & b \end{pmatrix}; \qquad \mathbf{R}(A'') = \begin{pmatrix} 0 & c \\ c & 0 \end{pmatrix}, \tag{1}$$

A'-modes appearing under the (x,x) and (y,y) configurations refer to tensor components a and b, respectively. A''-modes appearing under the (y,x) or (x,y) polarization configurations both refer to tensor component c. The difference in the two possible A' scattering configurations (components a, b) results from the fact that the surface unit cell is anisotropic, with the In chains extending along the $[1\bar{1}0]$ direction. Raman spectra shown in the following correspond in this notation to tensor component a.

We would like to note that in case of the hexagonal (8×2) reconstruction presented in Fig. 4(a) the C_S symmetry is lifted and the A'/A'' notation scheme is no longer applicable. A clear distinction between A' and A'' is not valid for hexagon structure.

3.3 Surface phonon modes of In-nanowire terminated Si(111) Due to the large penetration depth of light, the experimentally recorded Raman spectra are a superposition of bulk and surface phonon excitations. However, the Raman scattering cross-section depends significantly on the resonance of incident and scattered light with electronic states [20]. Surface phonons couple predominantly to surface electronic states [21]: as the atomic displacements related to surface phonons are confined to few topmost atomic layers, the deformation potential scattering is mediated by surface electronic states. Similarly, bulk modes scatter predominantly via the bulk electronic states. For the Raman experiments on Si a bulk resonance occurs at the E_1-bulk critical point of 3.4 eV [22]. Surface phonons are favourably recorded at lower energies under surface resonant conditions, using exiting laser lines close to the surface electronic transitions. Surface phonon modes have been measured for the (4×1) and (8×2) phases with HREELS at 300 and 90 K, respectively. A mode at 60 meV (484 cm^{-1}) was observed for the (4×1) phase, and two modes at 61 meV (492 cm^{-1}) and 33 meV (266 cm^{-1}) were observed for the (8×2) (see Table 1) [23].

Surface Raman spectroscopy reproduces these modes and reveals many additional ones. Raman spectra of (8×2) and (4×1) reconstructions are shown in Fig. 5. Strong modes at 435 and 59 cm^{-1} as well as weaker modes at 33, 65, 150, 474, and 493 cm^{-1} are observed for the (4×1) surface. The surface phonon modes are grouped in two distinct frequency regions: in the low frequency range, up to 100 cm^{-1}, the surface vibrational modes involve mainly displacements of the In atoms of the outer atomic layer; the higher frequency modes above 250 cm^{-1} involve, in contrast, mainly displacements of the Si atoms in between

Table 1 Overview of A' surface phonon modes, in cm^{-1}, measured for both phases at 30 K. The line width of a mode is given in brackets. The energy difference for the (4×1)-mode at $484\,cm^{-1}$ visible with HREELS is due to a temperature related shift, since the (4×1) HREELS data were taken at 300 K.

(4×1)		$(4 \times$ '2')	
RS (30 K)	HREELS[23]	RS (30 K)	HREELS[23]
33(20)	–	33(3)	–
–	–	45(2)	–
59(3)	–	60(6)	–
65(18)	–	–	–
146(50)	–	142(12)	–
–	–	158(15)	–
–	–	266(8)	266
–	–	415(8)	–
435(10)	–	435(13)	–
–	–	459(11)	–
474(11)	–	474(14)	–
493(12)	484	493(15)	492

and underneath the In-adsorbate structure. Both kinds of surface modes are separated in frequency since the atomic mass of In (115 amu) is much larger than that of Si (28 amu).

On formation of the LT phase, significant differences in the spectra were observed, especially in the low frequency region. Very sharp modes appear at 33 and $45\,cm^{-1}$, while the mode at $65\,cm^{-1}$ cannot be distinguished anymore. At higher energies new modes are observed at 266, 415 and $459\,cm^{-1}$. Thus, the formation of the LT phase is accompanied by the retention of the RT phase modes at similar intensities and frequencies (which is an unusual observation) and the appearance of new modes in the immediate vicinity of the RT phase modes.

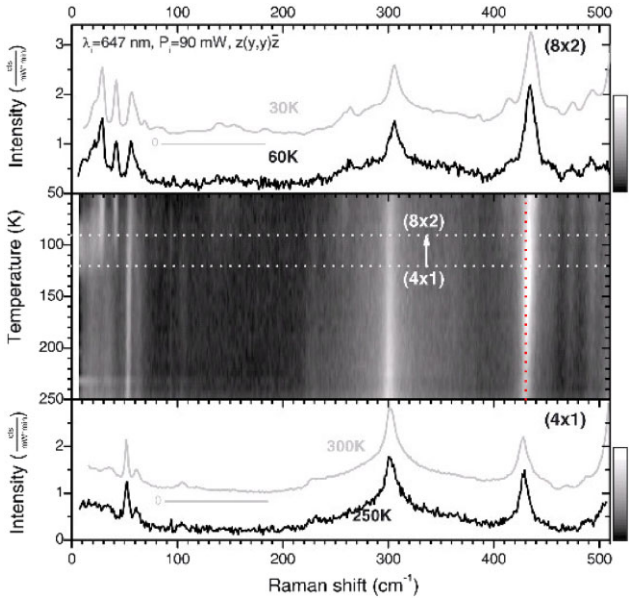

Figure 5 (online colour at: www.pss-b.com) Comparison of Raman spectra of the (4×1) (lower panel) and $(8 \times 2)/(4 \times 2)$ (upper panel) phases. Spectra taken during the phase transition are shown in the middle panel as a temperature dependent Raman intensity pattern. Below 120 K additional modes appear for the $(8 \times 2)/(4 \times 2)$ phase. The bulk Si TO mode at $520\,cm^{-1}$ is not shown since it is ~500 times more intense than shown phonon modes. Measurements were taken at 647 nm and incoming and scattered polarization along $[01\bar{1}]$ direction ($E_i \parallel E_s \parallel [01\bar{1}]$). (Figure from Ref. [13]).

As there are a large number of vibrational modes detected a comparison with theoretical calculations based on competing In/Si reconstruction models could be very useful distinguishing between the various models. In an *ab initio* DFT-GGA-calculation by Bechstedt et al. [24] the surface phonon modes of the In-Si(111) (4×1) structure were addressed. Surface modes of A' and A'' symmetry were identified and eigenfrequencies as well as displacement patterns determined.

Based on the displacement patterns the modes were characterized as surface phonons and surface resonances involving mainly In–In, In–Si or Si–Si-vibrations (see Table 2). The calculation shows that in fact the low frequency modes are associated with In–In and the high frequency modes with Si–Si-displacements. However, no one-to-one correspondence between observed and calculated modes can be established since the eigenfrequencies of most of the modes differ significantly. One of the reasons for such a discrepancy could be the fact that the surface atoms move in a highly anharmonic potential due to the broken symmetry on the surface. This applies especially to the A' modes where the vibrations have a strong component perpendicular to the surface.

Unfortunately, no calculations for the (8×2) phase are available. However, some basic considerations could be done in respect to the number of vibrational modes in the (4×2) and (8×2) phases. A doubling of the surface unit cell induced by small changes in the atomic positions (distortions in the chain geometry as indicated in Fig. 1) would give rise to backfolding of the surface phonon branches within the reduced SBZ. As the phonon branches are expected to show dispersion, the backfolding would lead to the appearance of new phonon modes at the centre of the SBZ, with the original modes being retained at an unchanged energy. The modes at 33 and $45\,cm^{-1}$, 415 and $435\,cm^{-1}$, together with the separation of the $150\,cm^{-1}$ mode into two, support this interpretation. This interpretation is based on the assumption that the atomic configurations of (4×1) and (8×2)

Table 2 Symmetry, character and eigenfrequency of calculated surface modes (from Ref. [24]).

character	A' (cm^{-1})	A'' (cm^{-1})
In surface mode	31, 42, 54	21, 55
In/Si surface mode	104, 109	79
In/Si resonance mode	93, 129	51
Si/Si resonance mode	140, 303, 314, 394	81, 109
Si surface mode	255, 411	421

reconstructions are very similar [25]. However, the larger number of (8 × 2) surface modes as compared to the (4 × 1) structure is no surprise and is not necessarily a result of a simple distortion of the (4 × 1) chain like to (8 × 2) chain like reconstruction. This could be explained by the increase of the number of atoms in the SBZ which applies also to the (8 × 2) hexagonal reconstruction model since by the enlargement of the surface unit mesh from (4 × 1) to (8 × 2) the number of atoms per unit cell rises by the factor of four. In the outermost atomic layer, the (4 × 1) cell contains 4 In and 2 Si atoms, the (8 × 2) 16 In and 8 Si atoms. Since the total number of modes is given by three times the number of atoms per unit cell, we may expect even more surface modes to exist than those identified in the present set of spectra. The lower number of identified modes could be due to the relation between the Raman cross-section (including resonance) of the individual modes and spectral resolution. In particular broad modes may consist of a superposition of eigenmodes.

3.4 Resonant Raman scattering on In/Si(111) Here we discuss such Raman spectra taken with different laser lines energies [data in Fig. 6(a) from Ref. [13]]. Clearly, one recognizes the different scattering intensities when the excitation photon energy is changed. For a quantitative discussion the scattering intensities should be evaluated in terms of the scattering efficiencies, as a function of laser photon energy in order to eliminate all experimental parameters depending on photon energy.

In principle absolute values of the scattering efficiency can be obtained in that way. However, the whole procedure is very cumbersome and highly inaccurate, because of the different photometric measurements involved. This concerns first of all the incident power and the scattered power which often differ by up to 10 orders of magnitude and have to be measured with different detectors. More convenient is therefore if one can normalize in the same experiment with the scattering of a phonon whose scattering cross-section is known (*e.g.* substrate phonon) and eliminate in such a way the laser power dependence. In the case of the In/Si(111) surface the TO phonon of bulk silicon can be taken for that purpose

$$\frac{I_{\mathrm{surf}}}{I_{\mathrm{Si,TO}}} S_{\mathrm{Si,TO}} \sim S_{\mathrm{surf}}, \tag{2}$$

where S_{surf} then gives a quantity proportional to the desired Raman scattering efficiency of the surface modes.

Figure 6 compares spectra with normalized intensities $I/I_{\mathrm{Si,TO}}$ and amplitudes of some modes corrected for penetration depth and the resonance of the silicon bulk mode.

By analyzing the corrected spectra, the Raman susceptibilities for all modes can be plotted *versus* the incident photon energy [Fig. 6(b)] for the various modes. It can be easily seen that most surface phonon modes are resonant around 2 eV – the same energy where also the strongest anisotropy in the reflectance of the surface occurs (Fig. 3 and Refs. [26, 27]). Only the mode at 61 cm^{-1}, shows a different

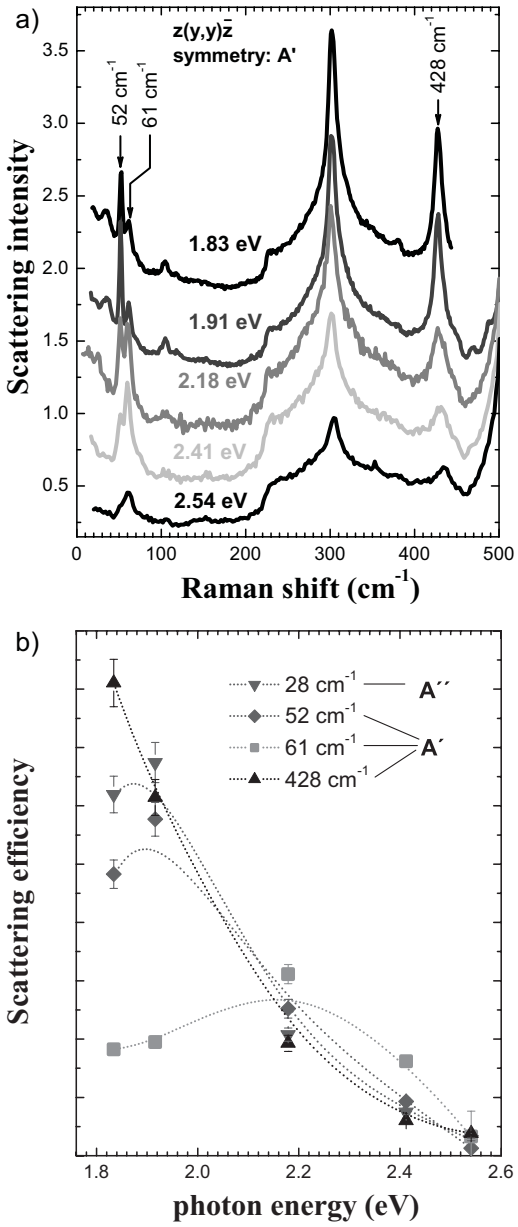

Figure 6 Resonance Raman scattering from Si(111)-In:(4 × 1). (a) Raman spectra normalized with the TO phonon intensity for various incident photon energies. The polarization vector *y* is [110] *e.g.* perpendicular to direction of the indium chains. The spectra are displaced vertically for better visibility. (b) Relative scattering efficiencies plotted *versus* incident photon energy for different phonons. The efficiencies of the A'' mode at 28 cm^{-1} were obtained from a different set of Raman spectra taken in $z(xy)\bar{z}$ polarization.

resonance at 2.2 eV. This different behaviour must be related to this particular A' -phonon which possibly couples to other electronic states than those modes resonantly enhanced in the red spectral region. To understand this in detail more theoretical information on the electronic states, particularly their localization on certain atoms and a comparison to the individual displacement patterns of the phonon modes must be available.

4 Summary In conclusion, we have compared the experimental and theoretical results for optical anisotropy and vibrational properties of the In/Si(111)(4×1)–(8×2) phase transition. We identified surface phonon modes for indium-nanowire terminated Si(111) surfaces by surface resonant Raman spectroscopy. It was found that the phonon–electron resonances are located at $\sim$2 eV, the energy where the largest optical anisotropy was observed. The eigenfrequencies of the surface phonons were analysed and compared to DFT results. The appearance of new surface phonon modes upon phase transition into the (8×2) surface phase is attributed to the increased size of the SBZ. The agreement between experimental data and theoretical calculations for the LT phase optical anisotropy gives strong evidence for the hexagonal reconstruction model. The structural changes upon the phase transition into the (8×2) structure in the view of vibrational properties are still under discussion.

Acknowledgements We thank C. Roland and I. Fischer for technical assistance. The financial support by the "Senatsverwaltung für Wissenschaft, Forschung und Kultur des Landes Berlin" and the "Bundesministerium für Bildung, Wissenschaft, Forschung und Technologie", by Science Foundation Ireland (SFI) under Contract No. 06/RFP/PHY042, and by NANOCHARM project is also gratefully acknowledged.

References

[1] S. Wang, W. Lu, W. G. Schmidt, and J. Bernholc, Phys. Rev. B **68**, 035329 (2003).
[2] C. González, J. Ortega, and F. Flores, New J. Phys. **7**, 100 (2005).
[3] H. Nienhaus, Phys. Rev. B **56**, 13194 (1997).
[4] H. Ibach and D. L. Mills, Electron Energy Loss Spectroscopy and Surface Vibrations (Academic Press, New York, 1982).
[5] G. Benedek and J. P. Toennies, Surf. Sci. **299**, 587 (1994).
[6] E. Hulpke (ed.), Helium Atom Scattering from Surfaces, Springer Series in Surface Science Vol. 27 (Springer, Berlin, 1992).
[7] W. Kress and F. W. de Wette, Surface Phonons Vol. 21 (Springer, Berlin, 1991).
[8] N. Esser, M. Köpp, P. Haier, and W. Richter, J. Electron Spectrosc. **64/65**, 85 (1993).
[9] K. Hinrichs, A. Schierhorn, P. Haier, N. Esser, W. Richter, and J. Sahm, Phys. Rev. Lett. **79**, 1094 (1997).
[10] M. Hünermann, J. Geurts, and W. Richter, Phys. Rev. Lett. **66**, 640 (1991).
[11] N. Esser and W. Richter, Raman Scattering from Surface Phonons, in: Topics in Applied Physics, Vol. 76, edited by M. Cardona and G. Guentherodt (Springer, Berlin, Heidelberg, New York, 2000).
[12] N. Esser, K. Hinrichs, J. R. Power, W. Richter, and J. Fritsch, Phys. Rev. B **66**, 075330 (2002).
[13] K. Fleischer, S. Chandola, N. Esser, W. Richter, and J. McGilp, Phys. Rev. B. **76**, 205406 (2007).
[14] K. Fleischer, S. Chandola, N. Esser, W. Richter, and J. F. McGilp, Phys. Status Solidi A **188**, 1411 (2001).
[15] X. López-Lozano, A. Krivosheeva, A. A. Stekolnikov, L. Meza-Montes, C. Noguez, J. Furthmüller, and F. Bechstedt, Phys. Rev. B **73**, 035430 (2006).
[16] S. Wippermann and W. G. Schmidt, Surf. Sci. **603**, 247 (2009).
[17] S. Chandola, K. Hinrichs, M. Gensch, N. Esser, S. Wippermann, W. G. Schmidt, F. Bechstedt, K. Fleischer, and J. F. McGilp, Phys. Rev. Lett. **102**, 226805 (2009).
[18] P. H. Hahn, W. G. Schmidt, and F. Bechstedt, Phys. Rev. Lett. **88**, 016402 (2001).
[19] A. A. Stekolnikov, F. Bechstedt, and W. G. Schmidt, Phys. Rev. Lett. **98**, 026105 (2007).
[20] M. Cardona and G. Güntherodt (eds.), Light Scattering in Solids II, Topics in Applied Physics, Vol. 50 (Springer, Berlin, Heidelberg, New York, 1982).
[21] P. V. Santos, N. Esser, M. Cardona, W. G. Schmidt, and F. Bechstedt, Phys. Rev. B **52**, 12158 (1995).
[22] A. Compaan and H. J. Trodahl, Phys. Rev. B **29**, 793 (1984).
[23] K. Sakamoto, H. Ashima, H. W. Yeom, and W. Ushida, Phys. Rev. B **62**, 9923 (2000).
[24] F. Bechstedt, A. Krivosheeva, J. Furthmüller, and A. A. Stekolnikov, Phys. Rev. B **68**, 193406 (2003).
[25] K. Fleischer, S. Chandola, N. Esser, W. Richter, and J. F. McGilp, Phys. Rev. B **67**, 235318 (2003).
[26] F. Pedreschi, J. D. OMahonya, P. Weightman, and J. R. Power, Appl. Phys. Lett. **73**, 2152 (1998).
[27] K. Fleischer, S. Chandola, N. Esser, W. Richter, J. F. McGilp, W. G. Schmidt, S. Wang, W. Lu, and J. Bernholc, Appl. Surf. Sci. **234**, 302 (2004).